Electronic Supplementary Material (ESI) for Journal of Materials Chemistry C.
This journal is © The Royal Society of Chemistry 2020

Highly Stretchable and Sensitive Strain Sensors based on Carbon Nanotubes-Elastomer Nanocomposites: The Effect of Environmental Factors on Strain Sensing Performance

Mohammad Nankali[1], Norouz Mohammad Nouri[1,*], Mahdi Navidbakhsh[1], Nima Geran Malek[1], Mohammad Amin Amindehghan[1], Abdolsamad Montazeri Shahtoori[1], Marita Karimi[1], Morteza Amjadi[2,*]

[1]*School of Mechanical Engineering, Iran University of Science and Technology, Tehran, Iran*

[2]*Institute of Mechanical, Process and Energy Engineering, Heriot-Watt University, Edinburgh, UK*

Supporting Information

Corresponding authors: m.amjadi@hw.ac.uk and mnouri@iust.ac.ir

EDS spectrum and SEM mapping

To explore the composition and homogeneity of the coated CNT thin film, we conducted EDS spectroscopy and SEM mapping of the top surface of the CNTs-PDMS nanocomposite layer. As depicted in the inset of Figure S1, there is a uniform distribution of carbon elements in the SEM mapping, proving that all CNTs are uniformly distributed in the PDMS matrix. This is mainly due to the vacuum filtration process, where the local permeation rate of the nanoporous membrane decreases gradually by the accumulation of CNTs, automatically tuning the deposition rate. Hence, the homogeneity of the resulted CNTs film is guaranteed during the vacuum filtration.

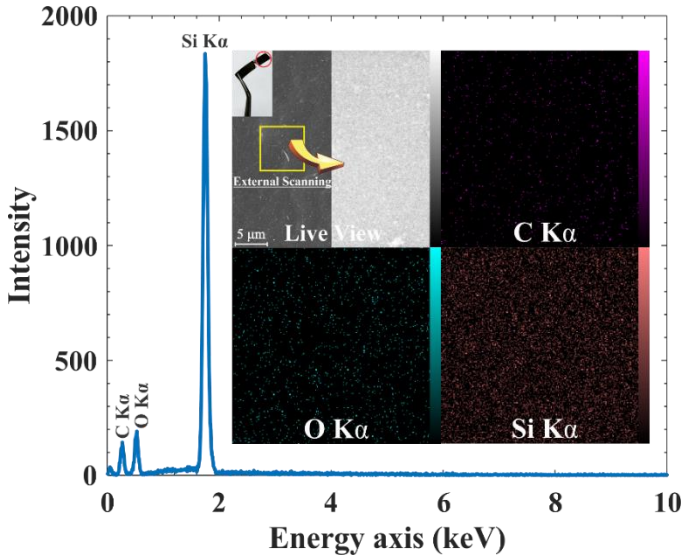

Fig. S1 EDS spectrum of the CNTs-PDMS nanocomposite film; insets, SEM mapping of the elemental distribution.

Viscoelastic properties

In order to evaluate the viscoelastic properties, dynamic mechanical properties of both PDMS film and strain sensor were investigated as below:

$$\sigma = \sigma_0 \sin(\omega t + \delta) \rightarrow \sigma = \sigma_0 \sin \omega t \cos \delta + \sigma_0 \cos \omega t \sin \delta \quad (1)$$

$$\varepsilon = \varepsilon_0 \sin \omega t \quad (2)$$

where σ and ε are dynamic stress and strain, respectively. ω is the frequency of sinusoidal oscillation, t is time, and δ is the phase lag between stress and strain. This phase lag is due to the excess time necessary for molecular motions and relaxations to occur. Also, σ_0 is the maximum stress applied and ε_0 is the strain at the maximum stress. Using equations (1) and (2), phase lag in elastic and viscous materials can be calculated as equations (3) and (4), respectively.

$$\sigma(t) = E\varepsilon(t) \rightarrow \sigma_0 \sin(\omega t + \delta) = E\varepsilon_0 \sin \omega t \rightarrow \delta = 0 \quad (3)$$

$$\sigma(t) = K\frac{d\varepsilon}{dt} \rightarrow \sigma_0 \sin(\omega t + \delta) = K\varepsilon_0 \omega \cos \omega t \rightarrow \delta = \frac{\pi}{2} \quad (4)$$

In viscoelastic materials like PDMS, a single modulus breaks into two terms: one related to the storage of energy and indicates the elastic behavior of the polymer (its spring-like nature), while another is related to the loss of energy or viscous behavior. The storage modulus (E'), also called the elastic or real modulus, measures the stored energy and is related to the sample's elastic behavior. The amount of energy lost due to the internal friction and motions is expressed as the loss modulus (E''), also called viscous or imaginary modulus. These two parameters are defined as follows:

$$E' = \frac{\sigma_0}{\varepsilon_0} \cos \delta \quad (5)$$

$$E'' = \frac{\sigma_0}{\varepsilon_0} \sin \delta \quad (6)$$

The ratio of the loss to the elastic modulus is called $\tan \delta$ or damping factor. This property is independent of geometrical effects and indicates how efficiently the material loses energy to

molecular rearrangements and internal friction under cyclic loading. This parameter varies with the state of the material, its temperature, and loading frequency.

$$tan\,\delta = \frac{E''}{E'} \tag{7}$$

According to Figure S2a and S2b, the storage modulus of both PDMS film and strain sensor suddenly dropped right after the glass transition temperature (T_g) of around -113.6 ℃, while the loss modulus has been maximized. It can be seen that at a small temperature interval, about 10 degrees above T_g, storage modulus has been declined about 30 to 35 times. Schneider *et al*. measured the elastic modulus of the PDMS elastomer at a constant ambient temperature for low strains ($\varepsilon < 45$ %) as 1.76 MPa.[1] Wu *et al.* reported an average elastic modulus of 1.71 MPa and 2.34 MPa for the CNTs-PDMS nanocomposites containing 1 and 4 wt.% of CNTs, respectively.[2] We evaluated the PDMS modulus in a wide temperature range from -150 to 170 ℃. According to the Figure S2a, the elastic modulus of the PDMS film (strain sensor) in the temperature range of -30 to 30 ℃ has changed from 2.43 to 1.43 MPa (3.25 to 1.59 MPa), respectively.

In order to represent the effects of CNT filers on the improvement of elastic modulus and the amount of energy lost during internal friction and motions at different temperatures, coefficients α and β were defined as equations (8) and (9).

$$\alpha = \left[\frac{E'_{Strain\ sensor} - E'_{PDMS\ Film}}{E'_{PDMS\ Film}}\right] \times 100 \tag{8}$$

$$\beta = \left[\frac{E''_{Strain\ sensor} - E''_{PDMS\ Film}}{E''_{PDMS\ Film}}\right] \times 100 \tag{9}$$

According to Figure S2c, the CNTs added to PDMS has increased the elastic modulus in the whole temperature range of the test and has a peak point of about 67% at T_g. The modulus in the temperature range of 0 to 50 ℃ has been increased 23 to 33 % with an average of 28.8 %.

This implies the fact that adding CNTs to the elastic matrix can strengthen the elastic modulus even in high temperatures.

From Figure S2d, it can be inferred that adding CNTs to PDMS has increased the internal friction and energy loss. After T_g, the amount of energy loss is proportional to the temperature value.

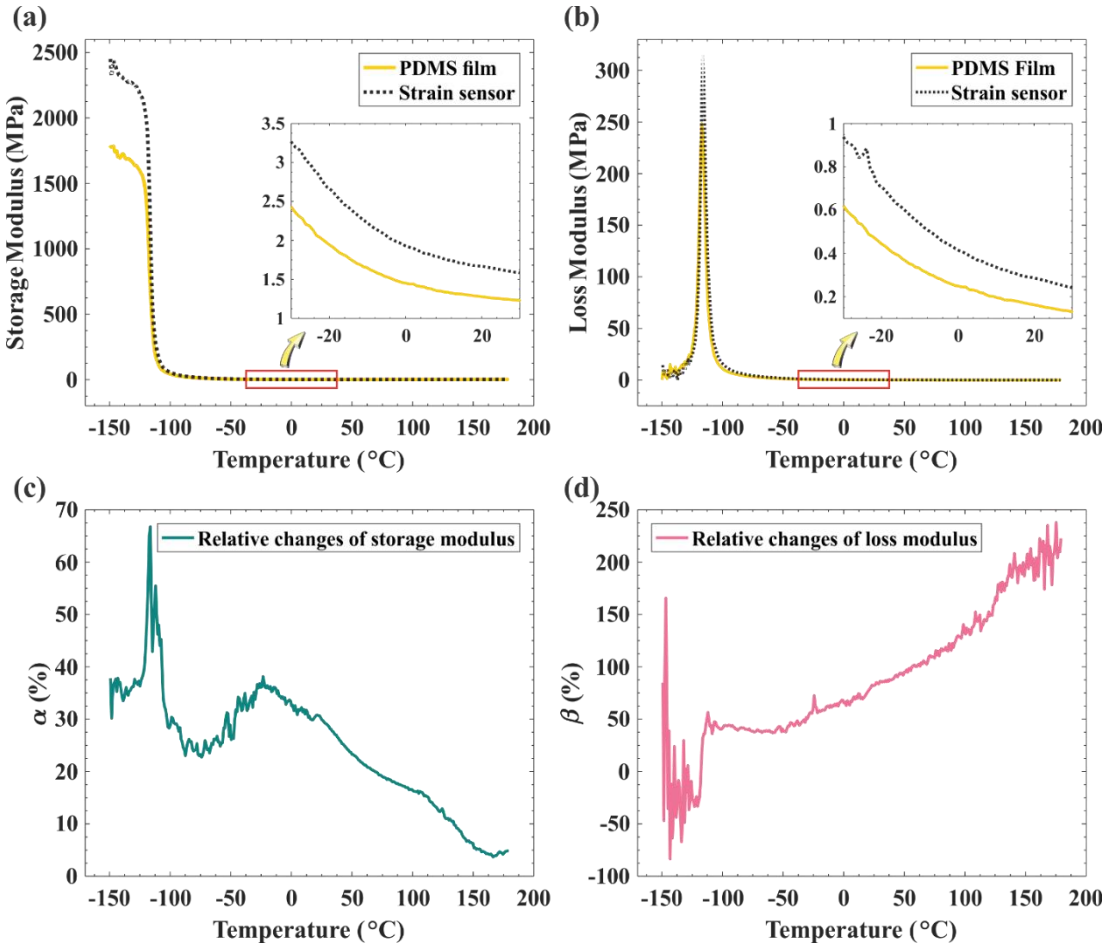

Fig. S2 (a) The storage modulus of a strain sensor and a pure PDMS film versus temperature. (b) The loss modulus of the strain sensor and pure PDMS film versus temperature. (c) Relative changes in the storage modulus versus temperature. (d) Relative changes in the loss modulus versus temperature.

Figure S3 illustrates $tan\,\delta$ of both strain sensor and pure PDMS film versus temperature. The loss tangent peaked at T_g for both samples, meaning that the effect of the thin CNT film on the overall T_g of the sensor is negligible (Table S1).

Table S1 The T_g and loss tangent for PDMS and strain sensor samples.

Sample	Glass transition temperature (℃)	Damping
PDMS film	-113.67	0.439
Strain sensor	-113.58	0.429

At temperatures below T_g, the damping factor for both samples dramatically decreased due to their purely elastic behavior. The trend was more prominent for the strain sensor sample, perhaps due to the reinforcement effect of the CNT film.

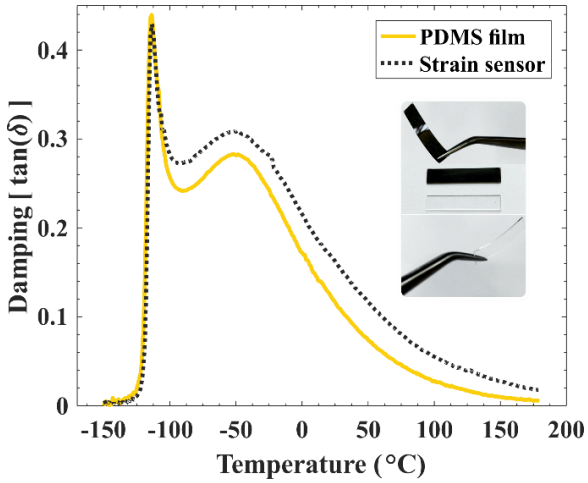

Fig. S3 Loss tangent of pure PDMS film and strain sensor samples versus temperature; insets, photographs of the pure PDMS film and strain sensor.

Percolation Theory

According to the 3D percolation theory, there is a power-law relationship for the electrical conductivity of composite materials as follows:

$$\sigma = \sigma_0 (V_f - V_c)^s \tag{10}$$

where V_f is the volume fraction of the filler and V_c is the volume fraction at the percolation threshold. The first parameter, V_f, can be represented as a function of tensile strain.[3] σ_0 is the electrical conductivity of the filler ($\sigma_0 = 1 \times 10^6\ S/m$)[4] and s is a fitting factor ($s = 2.38$). Our strain sensor is an ultrathin rectangular film with the length × width × thickness of 35 mm × 6 mm × 1.5 μm. When the strain is applied, a volumetric strain changes the volume as follow:

$$V_0 = l_0 \times t_0 \times w_0 \tag{11}$$

$$\begin{cases} \varepsilon_V = \dfrac{\Delta V}{V_0} \rightarrow V_1 = V_0 \varepsilon_V + V_0 = V_0 (1 + \varepsilon_V) \\ \varepsilon_V = \varepsilon_x + \varepsilon_y + \varepsilon_z = \varepsilon_x - \upsilon \varepsilon_x - \upsilon \varepsilon_x = \varepsilon_x (1 - 2\upsilon) \end{cases} \tag{12}$$

$$\rightarrow V_1 = V_0 \big(1 + \varepsilon_x (1 - 2\upsilon)\big) \tag{13}$$

For the volume fraction of the filler (V_f):

$$V_f = \frac{V_{CNTs}}{V_1} = \frac{V_{CNTs}}{V_0 \big(1 + \varepsilon_x (1 - 2\upsilon)\big)} \tag{14}$$

In equation (14), V_f is as a function of the applied strain. According to the literature, the Poisson's ratio of PDMS can be varied from $\nu = 0.4$ to $\nu = 0.495$, depending on the curing condition and the weight ratio of the cross-linker.[5-8] On the other hand, the Poisson's ratio of Multi-Walled CNTs is about $\nu = 0.1$.[9] Therefore, adding the randomly oriented CNTs to the PDMS matrix can further decrease the overall Poisson's ratio of the CNTs-PDMS nanocomposite. Consequently, we assumed the Poisson's ratio of the CNTs-PDMS nanocomposite as $\nu_{CNTs-PDMS} = 0.4$.[10] The volume fraction at the percolation threshold (V_c) is the final parameter, which we achieved experimentally in our previous article ($V_c = 0.096$).[11]

Figure S4 compares the conductivity of the strain sensor for strains up to 15%, showing a great agreement between experimental and theoretical data.

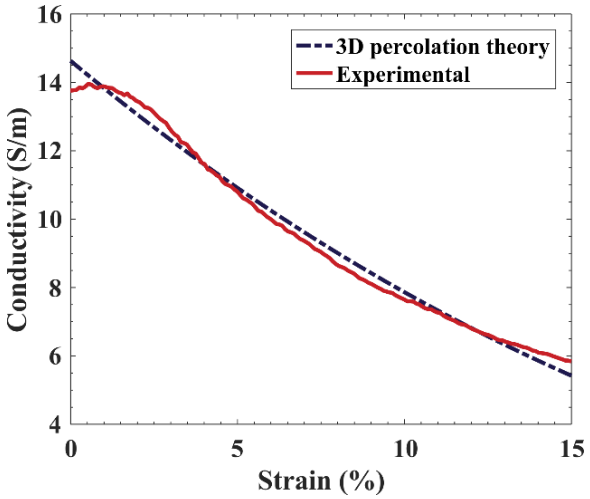

Fig. S4 Measured conductivity of a strain sensor versus the calculated conductivity based on the 3D percolation theory.

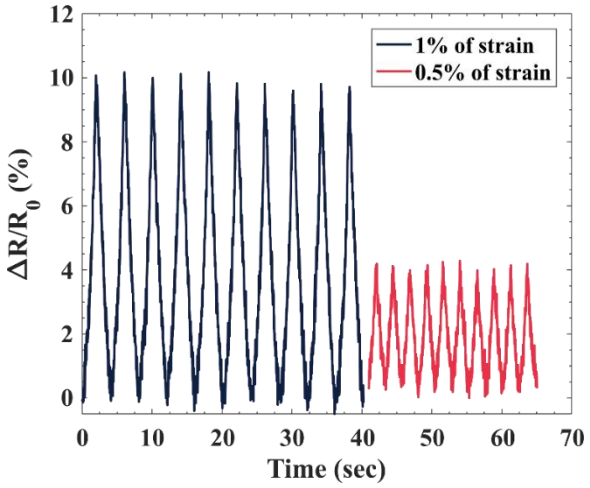

Fig. S5 Response of a strain sensor to small deformations (0.5 and 1% strains).

System time constant

Due to the fact that the strain sensor is a system with storage or dissipative capabilities, but negligible inertial forces, it can be modeled using a first-order differential equation as below:

$$a_1\dot{y} + a_0 y = F(t) \xrightarrow{dividing\ through\ by\ a_0} \tau\dot{y} + y = KF(t) \tag{15}$$

The parameter $\tau = a_1/a_0$ is the time constant of the system. Physically, a sudden change in loading (applied strain) can be used as the step input, which helps to obtain information about the time response of the system. The step function can be defined as:

$$\begin{cases} AU(t) = 0 \ \ t \leq 0^- \\ AU(t) = A \ \ t \geq 0^+ \end{cases} \tag{16}$$

where *A* is the amplitude, and *U(t)* is the unit step function. Setting $F(t) = AU(t)$ in equation (15) with an arbitrary initial condition $y(0) = y_0$ and solving for $t \geq 0^+$ yields

$$y(t) = KA + (y_0 - KA)e^{-t/\tau} \tag{17}$$

The solution $y(t)$ is the time response of the system which consists of steady-state (KA) and transient responses ($(y_0 - KA)e^{-t/\tau}$). Calling $y_\infty = KA$ as the steady response, the equation (17) can be rewritten in the following form:

$$\Gamma(t) = \frac{y(t) - y_\infty}{y_0 - y_\infty} = e^{-t/\tau} \tag{18}$$

The term $\Gamma(t)$ is called the error fraction of the output signal. Equation (18) is equivalent to the below transformation:

$$ln\Gamma = -(1/\tau)t \tag{19}$$

Which is of the linear form, $Y = mX + B$ (where $Y = ln\Gamma$, $m = -(1/\tau)$, $X = t$, and $B = 0$ here). A linear curve fitting through the experimental data provides a reasonable estimate of the slope, *m*, and yields the estimation of the system time constant (τ).

Environmental test setups

The performance of strain sensors at different temperatures (from ambient temperature to 65 °C) and relative humidity (RH) (from 30% to 95%) levels was investigated using the test setups shown in Figure S6. Figure S6a illustrates an insulated Styrofoam cooler-box used to create specific environments with controlled RH levels for the cyclic test setup. According to the figure, moisture enters the chamber through the red hose connected to the cold mist humidifier, and a ventilator is located inside the chamber to create uniform moisture conditions. The controlled temperature setup is shown in Figure S6b containing a programmable temperature chamber to create desired thermal conditions. Both temperature and humidity chambers have wire input/outputs on their sidewalls, allowing them to pass the electrical wires through the wall. Integrated digital temperature and humidity sensor (SHT31 from SENSIRION) was used to record the real-time temperature and humidity data in both chambers.

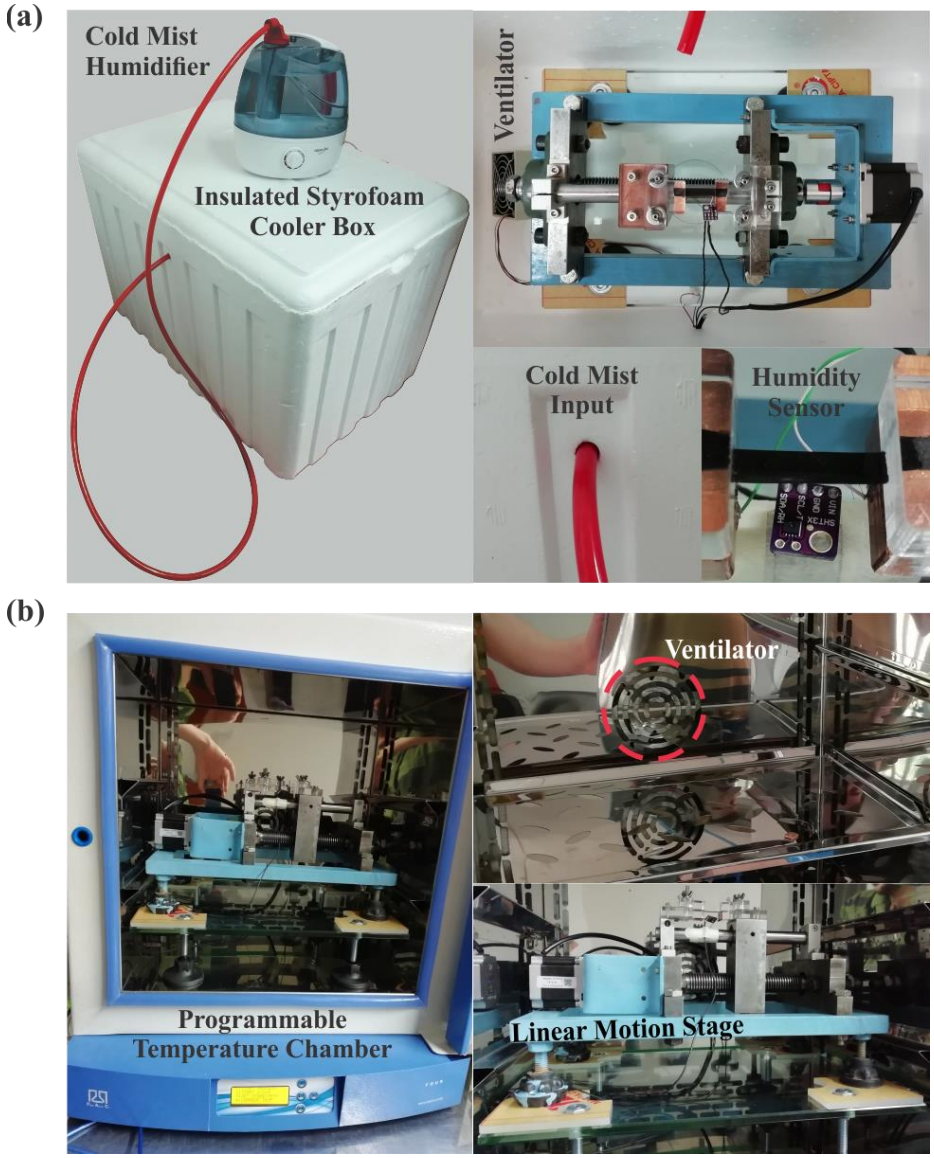

Fig. S6 (a) Humidity and (b) Temperature test setups.

Irreversible effects of humidity

The variations of base resistance of a strain sensor with temperature and RH are depicted in Figure S7a and S7b, respectively. Figure S7c shows the test results before and after the humidity test. After humidity tests in different RH levels, a strain sensor was rest in the environment for 48 and 72 hours and then tested again in the ambient condition. According to Figure S7c, the effects of humidity on the base resistance and strain sensing properties of the strain sensor is quite evident. These negative effects were irreversible and permanently changed the sensing behavior of the sensor.

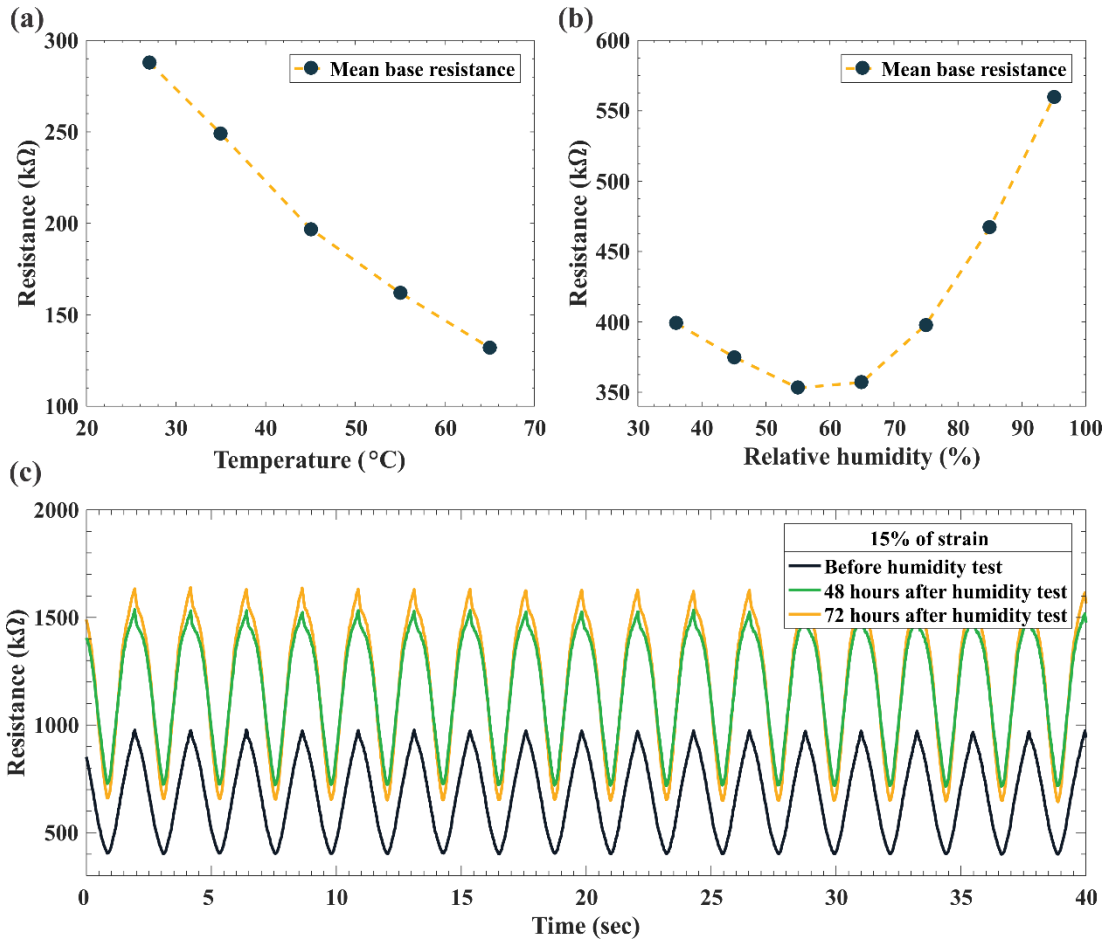

Fig. S7 (a) Base resistance of a strain sensor versus temperature change. (b) Base resistance of a sensor versus RH change. (c) Permanent changes in the piezoresistive behavior of a strain sensor before and after the humidity test, indicating irreversible effects of humidity on the piezoresistive properties of the strain sensor.

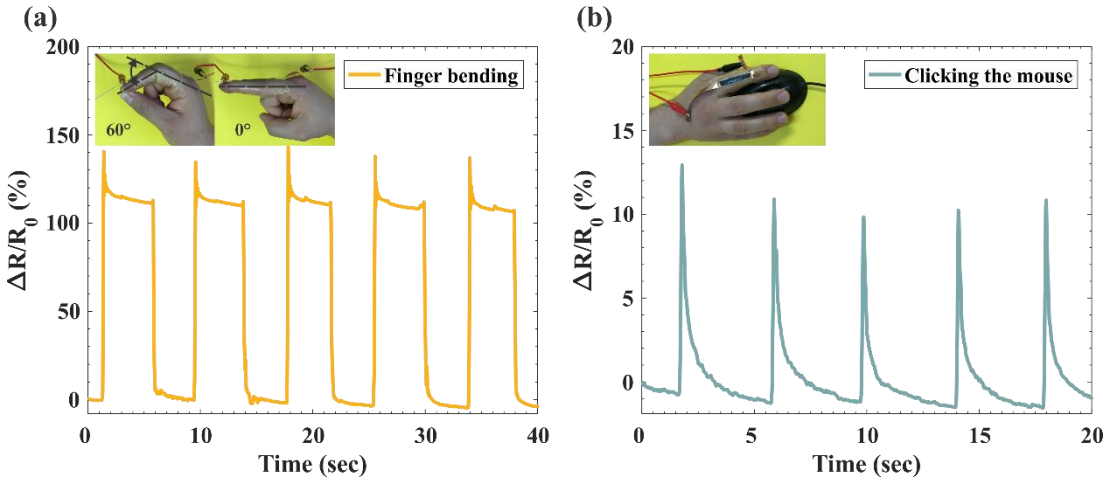

Fig. S8 (a) response of a strain sensor to finger bending movement; inset, photographs of the sensor attached to the index finger in relaxed and bent states. (b) response of a strain sensor while clicking a mouse; inset, photograph of the sensor while clicking the mouse.

Supplementary Movies:

Movie S1: Monitoring the deformation state of an air-inflated balloon (MP4).

Movie S2: Response of a strain sensor to holding-releasing a cup (MP4).

Movie S3: Application demonstration of the smart belt in respiration monitoring (MP4)

REFERENCES

1. F. Schneider, J. Draheim, R. Kamberger and U. Wallrabe, *Sens. Actuators, A*, 2009, **151**, 95-99.
2. C.-L. Wu, H.-C. Lin, J.-S. Hsu, M.-C. Yip and W. Fang, *Thin Solid Films*, 2009, **517**, 4895-4901.
3. M. Park, J. Im, M. Shin, Y. Min, J. Park, H. Cho, S. Park, M.-B. Shim, S. Jeon, D.-Y. Chung, J. Bae, J. Park, U. Jeong and K. Kim, *Nat. Nanotechnol.*, 2012, **7**, 803-809.
4. Y. Wang and G. J. Weng, in *Micromechanics and Nanomechanics of Composite Solids*, eds. S. A. Meguid and G. J. Weng, Springer International Publishing, Cham, 2018, pp. 123-156.
5. P. Gutruf, C. Zou, W. Withayachumnankul, M. Bhaskaran, S. Sriram and C. Fumeaux, *ACS Nano*, 2016, **10**, 133-141.
6. Y. Xia, E. Kim, X.-M. Zhao, J. A. Rogers, M. Prentiss and G. M. Whitesides, *Science*, 1996, **273**, 347.
7. S. Dogru, B. Aksoy, H. Bayraktar and B. E. Alaca, *Polym. Test.*, 2018, **69**, 375-384.
8. A. T. Sepúlveda, R. Guzman de Villoria, J. C. Viana, A. J. Pontes, B. L. Wardle and L. A. Rocha, *Nanoscale*, 2013, **5**, 4847-4854.
9. M. Talò, B. Krause, J. Pionteck, G. Lanzara and W. Lacarbonara, *Composites, Part B*, 2017, **115**, 70-78.
10. S. Xu, Z. Fan, C. Li, P. Wang, K. A. Sammed and L. Pan, *Carbon*, 2019, **155**, 421-431.
11. M. Nankali, N. M. Nouri, N. Geran Malek and M. A. Sanjari Shahrezaei, *J. Compos. Mater.*, 2019, **53**, 3047-3060.